TU Delft

Delft University of Technology

The importance of accounting for large deformation in continuum damage models in predicting matrix failure of composites

Tijs, B. H.A.H.; Dávila, C. G.; Turon, A.; Bisagni, C.

DOI
10.1016/j.compositesa.2022.107263

Publication date
2023

Document Version
Final published version

Published in
Composites Part A: Applied Science and Manufacturing

Citation (APA)
Tijs, B. H. A. H., Dávila, C. G., Turon, A., & Bisagni, C. (2023). The importance of accounting for large deformation in continuum damage models in predicting matrix failure of composites. *Composites Part A: Applied Science and Manufacturing*, *164*, Article 107263. https://doi.org/10.1016/j.compositesa.2022.107263

Important note
To cite this publication, please use the final published version (if applicable).
Please check the document version above.

Copyright
Other than for strictly personal use, it is not permitted to download, forward or distribute the text or part of it, without the consent of the author(s) and/or copyright holder(s), unless the work is under an open content license such as Creative Commons.

Takedown policy
Please contact us and provide details if you believe this document breaches copyrights.
We will remove access to the work immediately and investigate your claim.

This work is downloaded from Delft University of Technology.
For technical reasons the number of authors shown on this cover page is limited to a maximum of 10.

Composites: Part A 164 (2023) 107263

Contents lists available at ScienceDirect

Composites Part A

journal homepage: www.elsevier.com/locate/compositesa

The importance of accounting for large deformation in continuum damage models in predicting matrix failure of composites

B.H.A.H. Tijs [a,d,*], C.G. Dávila [b], A. Turon [c], C. Bisagni [d]

[a] Fokker/GKN Aerospace, Papendrecht, The Netherlands
[b] NASA Langley Research Center, Durability, Damage Tolerance and Concepts Branch, Hampton, USA
[c] University of Girona, AMADE, Polytechnic School, Girona, Spain
[d] Delft University of Technology, Faculty of Aerospace Engineering, Delft, The Netherlands

ARTICLE INFO

This paper is dedicated to the memory of our dear friend and colleague Claudio S. Lopes

Keywords:
Continuum damage model
Large shear deformations
Progressive failure
Ply splitting

ABSTRACT

The work presented in this paper investigates the ability of continuum damage models to accurately predict matrix failure and ply splitting. Two continuum damage model approaches are implemented that use different stress–strain measures. The first approach is based on small-strain increments and the Cauchy stress, while the second approach account for large deformation kinematics through the use of the Green–Lagrange strain and the 2nd Piola–Kirchhoff stress. The investigation consists of numerical benchmarks at three different levels: (1) single element; (2) unidirectional single ply open-hole specimen and (3) open-hole composite laminate coupon. Finally, the numerically predicted failure modes are compared to experimental failure modes at the coupon level. It is shown that it is important to account for large deformation kinematics in the constitutive model, especially when predicting matrix splitting failure modes. It is also shown that continuum damage models that do not account for large deformation kinematics can easily be adapted to ensure that the damage modes and failure strength are predicted accurately.

1. Introduction

The aviation sector is moving towards more sustainable and affordable aircraft structures, which requires changes to be made in the way aircraft structures are designed and manufactured. An example is the development of a thermoplastic composite fuselage [1,2] that makes use of new joining techniques such as thermoplastic welding. Although these new manufacturing techniques reduce the amount of mechanical fasteners required, they also make the strength of the structure more reliant on the matrix-dominated failure behavior of the thermoplastic material [3,4]. With the recent advancements in the ability to accurately predict composite failure modes, there is now the opportunity to develop predictive tools to evaluate the strength and failure behavior of these new structural concepts and fastener-free joints. However, accurately predicting matrix dominated failure, in particular ply splitting cracks, still poses a number of difficulties.

Simulating the failure mechanisms in composites using finite element analysis [5–9] is generally done through modeling cracks using either discrete or smeared approaches [10]. Examples of discrete approaches include the extended finite element method (X-FEM) [11], the discrete cohesive crack approach [12], and the floating-node method [13]. These methods are capable to predict both the intra- and inter-laminar damage mechanics with high accuracy, but generally at a high computational cost.

Maimí et al. [14] showed that cracks can also be represented in a more diffused manner by using a continuum damage mechanics (CDM) approach. In this case, crack propagation is represented by a softening law. Although softening results in a diffused crack unlike the real physical phenomenon at the micro-scale of the material, CDM provides an appealing framework to simulate the failure mechanisms at the meso-scale, as demonstrated by Lopes et al. [15] for various composite coupon tests in a virtual testing lab environment [16,17].

From experimental observations of matrix-dominated damage in unnotched [18] and notched composite specimens [19–24], it is apparent that ply splits, and their interaction with delaminations [22] play an important role in the failure mechanics of composite materials. To address these difficulties, Lopes et al. [15] extended the CDM formulation of Maimí et al. [14] to three dimensions and combined it with several key modeling aspects to allow the appropriate kinematic simulation of composites. These key modeling aspects include (1) ply-by-ply modeling using fiber-aligned meshes and directional biasing; (2) nonlinear shear and mesh size regularization; and (3) an advanced

* Corresponding author.
E-mail address: bas.tijs@fokker.com (B.H.A.H. Tijs).

https://doi.org/10.1016/j.compositesa.2022.107263
Received 5 August 2022; Received in revised form 30 September 2022; Accepted 9 October 2022
Available online 18 October 2022
1359-835X/© 2022 The Author(s). Published by Elsevier Ltd. This is an open access article under the CC BY license (http://creativecommons.org/licenses/by/4.0/).

element deletion scheme to guarantee solution robustness. Lopes et al. [15] also demonstrated that fiber-aligned meshes reduce the mesh-induced direction bias that is a source of mesh dependence in strain localization models. When fiber-aligned meshes are combined with large element aspect ratios, the mesh can direct matrix cracks to grow along the fiber direction, with the additional benefit of reducing computational cost [16]. However, it was found that rather large aspect ratios are required to prevent spurious failure modes and to achieve fully developed ply splits.

The difficulties of predicting ply splits with CDM models was also investigated by Leone [25], who developed a CDM methodology to represent the kinematics of matrix cracks in a deformable bulk material in accordance with the deformation gradient decomposition (DGD) methodology [25]. Leone [25] showed that CDM models, that do not account for large deformation kinematics, trigger spurious failure modes which make it difficult to predict ply splits. The DGD methodology, which does account for large deformation kinematics, is able to overcome this issue. Unfortunately, the use of these advanced CDM models may also come at a cost, as they generally rely on several internal convergence loops, for example to (1) search for the correct through-thickness crack angle; (2) solve nonlinear shear equations; or (3) achieve convergence in equilibrium between crack and bulk material displacements. Furthermore, predicting the final failure modes at the coupon level when many elements are nearly fully damaged requires special attention to the robustness of the continuum damage model to prevent unintended termination of the analysis, as addressed by Lopes et al. [15].

Composites may also exhibit significant nonlinear behavior, especially in matrix-dominated loading conditions. The nonlinear response may result from a number of geometrical and material related mechanisms. This includes plasticity in the matrix, fiber/matrix debonding, damage accumulation and reorientation of the fibers [26]. Lafarie-Frenot and Touchard [27] compared the in-plane shear behavior of thermoset versus thermoplastic composites and showed significant loss in shear stiffness and a nonlinear response for both materials. The thermoset composites reached shear strain values of approximately 5%, while the thermoplastic matrix showed a much more pronounce plastic behavior and failed at nearly 15% shear strain. The small degree of polymer deformation and the more brittle behavior of thermoset composites compared to thermoplastic composites can also be observed during interlaminar tests [28]. This is further confirmed by recent SEM micrographs of mode II interlaminar tests on thermoplastic composites presented by Tijs et al. [4], which feature significant polymer drawing out and extensive plastic deformation in the plane of the delamination.

The aim of this study is to investigate the influence of the different methodologies used in two recent continuum damage models [15,25] to accurately predict ply splitting, and to propose an efficient methodology to improve CDM models for this specific failure mode. This focus is chosen to improve the methodology for future use in thermoplastic composites and conduction welded joints, as this material will experience much larger deformations within the matrix-dominated failure modes. As part of the investigation, a dedicated CDM model was developed to investigate different approaches while keeping the implementation based on a simple and efficient two-dimensional (2D) failure criteria. The investigation consists of numerical benchmarks at three different levels. The implication of using the different approaches are highlighted at each level and the results are compared to experimental data. In the next section, the CDM models used herein are briefly described, followed by the analysis and discussion of the CDM models at three different levels: (1) single element; (2) unidirectional (UD) single ply open-hole specimen; and (3) open-hole composite laminate coupon.

2. CDM models

In this section, the different CDM models that are evaluated in this work are described. The first model, *CDM3D* [15,16], was developed in collaboration between IMDEA Materials Institute and Fokker/GKN Aerospace. The second model, NASA *CompDam*, is based on DGD [29]. The response of these models is compared to two CDM models specifically designed for this study. The models include approaches from both the *CMD3D* and the *CompDam* models to study (1) the influence of using small strain increments (*CDM-SS*) and (2) accounting for large deformation (*CDM-LD*) kinematics. All other aspects of the CDM implementation are the same to ensure that the general response of the CDM models remain identical. A summary of the different models and their naming is defined as follows:

- *CDM3D*: 3D Continuum Damage Model [15,16]
- *CompDam*: NASA CompDam DGD [29]
- *CDM-SS*: CDM based on Small Strain increments
- *CDM-LD*: CDM based on Large Deformation kinematics

CDM3D and *CDM-SS* are approaches that work well in situations where local deformations are not large, but they do not account for large deformation kinematics, while *CompDam* and *CDM-LD* are developed for geometrically nonlinear analysis. In addition to the aforementioned models, the Abaqus built-in Hashin model is also compared at the single element level. However, this model is not evaluated further as the response is similar to the other CDM models. All analyses were performed in Abaqus/Explicit [30].

2.1. CDM3D model

The CDM3D model takes into account the three-dimensional (3D) stress state through the physically-based 3D failure criteria proposed by Catalanotti et al. [31]. The implementation is described in full detail by Lopes et al. [15] and is originally based on the work of Maimí et al. [32] that guarantees the correct energy dissipation for each fracture mode in a composite material. The laminate compliance tensor, $[H(d_M)]$, is affected by the damage variables in each orthotropic direction $d_M (M = 1\pm, 2\pm, 3\pm, 4, 5, 6)$, as shown in Fig. 1, and is associated with the damage evolution laws for each failure mode. Each damage evolution law is defined by the strength $(X_t, X_c, Y_t, Y_c, S_L, S_T)$, fracture toughness (G_M), and element direction $(L = 1, 2, 3)$ of the corresponding failure mode, respectively in fiber longitudinal tension/compression (Fig. 1a), matrix transverse tension/compression (Fig. 1b), and matrix shear (Fig. 1c). Out-of-plane tension $(M = 3_+)$ is disabled and accounted for by the interlaminar model. The shear components follow elasto-plastic behavior defined by nonlinear relationships based on explicit forms of the Ramberg–Osgood law. Fiber failure is implemented using a superposition of cohesive laws to represent the different fiber failure modes such as fiber breakage, pull-out and kinking as proposed by Dávila et al. [33].

The corresponding compliance tensor with damage follows the Abaqus/Explicit convention and is expressed as:

$$[H(d_M)] = \begin{bmatrix} \frac{1}{(1-d_1)E_1} & -\frac{\nu_{12}}{E_1} & -\frac{\nu_{12}}{E_1} & 0 & 0 & 0 \\ -\frac{\nu_{12}}{E_1} & \frac{1}{(1-d_2)E_2} & -\frac{\nu_{23}}{E_2} & 0 & 0 & 0 \\ -\frac{\nu_{12}}{E_1} & -\frac{\nu_{23}}{E_2} & \frac{1}{(1-d_3)E_3} & 0 & 0 & 0 \\ 0 & 0 & 0 & \frac{1}{(1-d_6)G_{12}} & 0 & 0 \\ 0 & 0 & 0 & 0 & \frac{1}{(1-d_4)G_{23}} & 0 \\ 0 & 0 & 0 & 0 & 0 & \frac{1}{(1-d_5)G_{13}} \end{bmatrix} \quad (1)$$

An advantage of this approach is that the damage behavior of each orthotropic direction can be individually defined, but it also requires correct coupling of damage variables that may influence softening in a specific direction depending on the crack orientation. Related to this study, it is important to consider that the stress–strain measure in this model follows the CDM approach based on small strain increments.

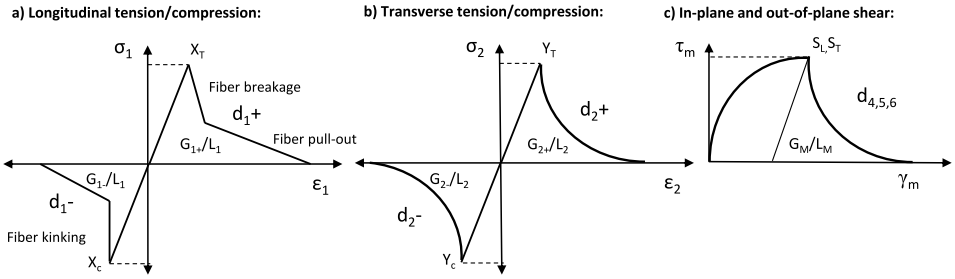

Fig. 1. CDM3D damage laws: (a) longitudinal tension/compression, (b) transverse tension/compression, (c) in-plane and out-of-plane shear.

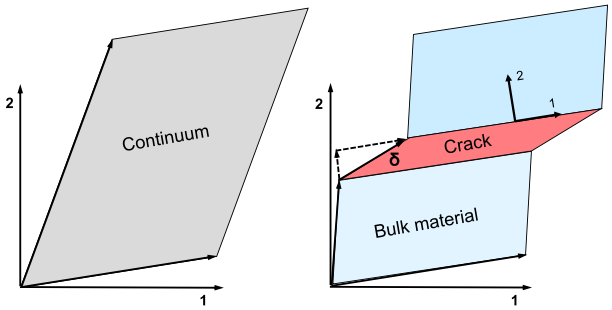

Fig. 2. CompDam DGD decomposition of crack and bulk material in a continuum element.

2.2. CompDam model

The CompDam model [29] was developed to accurately represent the kinematics of composite damage, and in particular for the simulation of matrix cracks formed under tension, compression, and shear loading conditions. The kinematics of a matrix crack are represented by treating them as a cohesive crack embedded in a deformable bulk material, and the relative contributions of the crack opening and bulk deformation are determined in accordance with the DGD methodology. The method uses additive decomposition of the deformation gradient tensor into 'bulk material' and 'crack' components as compared in Fig. 2 to a continuum during shear deformation. In the DGD methodology, the cohesive displacement-jump vector, δ, represents the deformation on an embedded cohesive crack. Matrix damage is accounted for in the embedded cohesive crack, while fiber damage is modeled using strain-softening, as shown in Fig. 1(b). Fiber damage is, as in *CDM3D*, based on superposition of cohesive laws. The shear components follow elasto-plastic behavior defined by nonlinear relationships based on the Ramberg–Osgood law, however, unlike *CDM3D*, this has to be solved using the Newton–Raphson method. The DGD methodology returns a single damage variable (d_2) for the softening behavior, which is coupled with the 3-direction depending on the crack orientation because the model can distinguish between a matrix crack and delamination.

An advantage of the DGD approach is that the damage of the continuum can be directly related to the orientation of the crack and mixed-mode conditions can be accurately derived from the crack opening displacement-jump. A disadvantage is that the methodology requires internal convergence loops to solve the displacement jumps, which may affect computational efficiency and solution robustness. Related to this study, it is important to consider that the stress–strain measure in this model accounts for large displacement in geometrically nonlinear problems in Abaqus/Explicit.

2.3. CDM-SS and CDM-LD models

The intralaminar CDM models in this study were implemented through a user-defined "VUMAT" subroutine using a numerically explicit integration scheme and are based on the Puck 2D failure criterion [34–36]. The failure criteria provides a closed-form solution for the fracture plane angle. Since an iterative procedure to determine the fracture plane angle is not required, this methodology is computationally efficient. The theory classifies lamina failure by Fiber Fracture (FF) and Inter-Fiber-Fracture (IFF), also referred to as fiber and matrix failure, respectively. Fiber failure in tension and compression follows a simple maximum stress formulation, while matrix failure is described by three failure modes. Failure due to matrix tension and/or in-plane shear is referred to as Mode A and results in a fracture plane angle equal to zero. The fracture angle remains at zero degree during moderate combined loading in shear and compression, identified as Mode B. As compressive loads increase, the fracture plane angle increases up to 54 degree in pure compression. This final fracture mode is identified as Mode C. The implemented version of the 2D Puck failure criteria follows the VDI-guideline VDI2014, Part 3 [37], which includes weakening of the matrix strength due to high fiber stresses [36].

After the onset of damage, strain-softening laws are used to damage the ply for each in-plane failure mode ($d_{1\pm}, d_{2\pm}, d_6$) as shown in Fig. 1. Softening in the fiber direction is implemented through the trilinear softening law of the CompDam implementation [29]. For matrix failure, the equations for exponential softening from Maimí et al. [32] are used to ensure that the computed dissipated energy is independent of mesh refinement. The maximum element size for each failure mode is calculated according to the crack band model [38], where the characteristic element length is calculated for a material-aligned meshing strategy following the modeling approach defined in Falcó et al. [16]. The damage and internal parameters are also used to allow for closure of transverse cracks under load reversal. Depending on the sign of the normal stress, a damage mode can be either activated or disabled. It is assumed that a tensile matrix crack (Mode A) can be closed in compression (Mode B), while shear cracks and cracks with fracture angles higher than 0° (Mode C) cannot be closed. Shear damage (d_6) is coupled by both fiber and matrix failure [32] in damaging the stiffness matrix. Frictional effects are not considered in the model.

Shear nonlinearity in the 1–2 plane is modeled using the Ramberg–Osgood equation based on the CompDam implementation [29], where the parameters are obtained from fitting experimental in-plane shear tests. The response is assumed to be plastic until the onset of damage, after which the element is damaged following an exponential softening

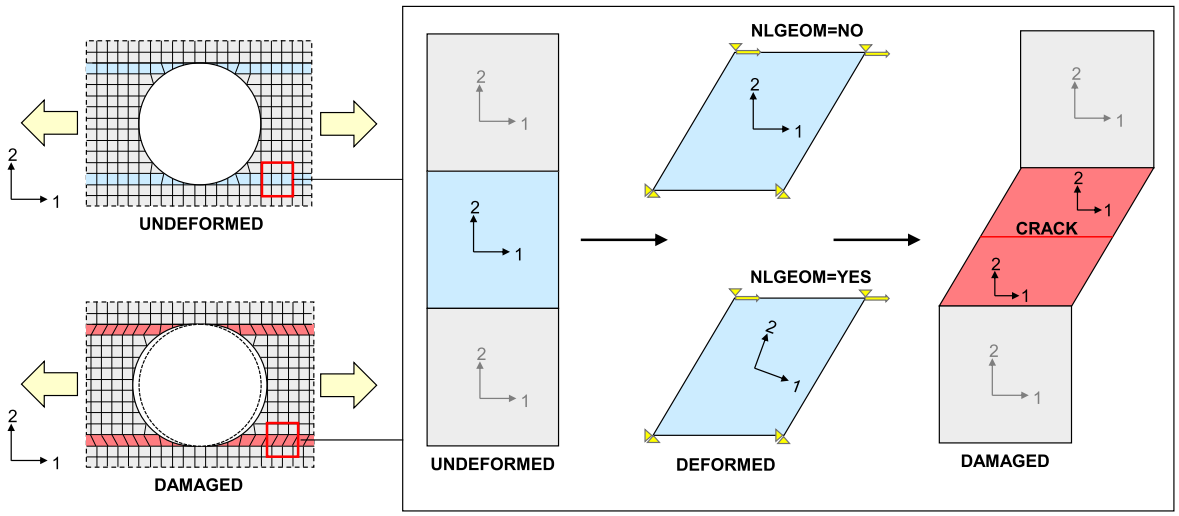

Fig. 3. Element deformation of Continuum Damage Model during ply splitting and default local coordinate system in Abaqus/Explicit.

law that is regularized according to the mode II fracture toughness. Nonlinear behavior in other directions is not considered. Finally, an element deletion strategy is implemented in order to avoid excessive element distortion which may significantly influence the runtime of the analysis or even crash it. These highly distorted elements generally exhibit sudden changes in volume that can be detected through the determinant of the deformation gradient $\det(\mathbf{F})$ [39]. The criteria for element deletion is adopted from Falcó et al. [16], and is set to be more strict during very large deformations. For fiber failure, the elements are deleted once the damage variable becomes nearly one ($d_{1\pm} \geq 0.99999$). Furthermore, the elements are also deleted if any of the strains becomes larger than one ($|\epsilon_i| \geq 1.0 (i = 1,2); \gamma_i| \geq 1.0 (i = 12)$). Finally, the elements are also deleted if large volume changes occur ($\det(\mathbf{F}) \leq 0.4$ or $\det(\mathbf{F}) \geq 4.0$). This strategy ensures that elements are only deleted if they are highly deformed or damaged and no longer carry any loads, as early deletion or limiting damage variables might influence the final failure modes.

The main difference between the two models presented in this study is related to the definition of the stress–strain measures and how the material axis rotates during geometrically linear and nonlinear analyses. During geometrically nonlinear analyses (NLGEOM=YES) the strain increment given by Abaqus/Explicit follows a co-rotational coordinate system where the material axis is rotated with the element, while for geometrically linear analyses this is not the case. An example of the material axis rotation during simple shear deformation for both cases is given in Fig. 3. The desired element deformation and crack orientation during the damaged state is also given. If the strain is derived following the material rotation in the deformed situation during geometrically nonlinear analyses, then the damaged compliance tensor, as described in Eq. (1), would also follow this rotation and may cause issues with incorrectly defined orientation of the softening directions. The incorrectly defined matrix crack orientation due to material axis rotation may cause load transfer across matrix cracks, where the strain and/or rotations due to softening and material nonlinearity may become large enough to invalidate the assumptions inherent to small strain theory. This can then trigger spurious secondary failure mechanisms such as fiber failure [25].

Both the approach of the *CDM3D* model and a simplified version of the large deformation approach of *CompDam* are implemented in the CDM in order to investigate if only accounting for large displacements and rotation on the element deformation would be sufficient to predict ply splitting. Both implementations are briefly explained next.

2.3.1. CDM-SS: CDM approach based on small strain increments

In CDM models [32], the presence of a crack is often accounted for by damaging the stiffness tensor, $\mathbf{C}$. The damaged stiffness tensor, $\mathbf{C^d}$, is used to calculate the stress, $\boldsymbol{\sigma}$, from the current strain, $\boldsymbol{\epsilon}$, without explicitly modeling the crack. The total strain, $\boldsymbol{\epsilon}$, is calculated by adding the strain increment, $\Delta\boldsymbol{\epsilon}$, given by Abaqus/Explicit to the total strain from the previous step for each time increment ($\boldsymbol{\epsilon} = \boldsymbol{\epsilon}_{prev} + \Delta\boldsymbol{\epsilon}$).

$$\boldsymbol{\sigma} = \mathbf{C^d} : \boldsymbol{\epsilon} \tag{2}$$

An alternative approach that yields the same result as using small strain increments is based on the logarithmic strain and Cauchy stress. The logarithmic strain tensor, $\mathbf{E}_{log}$, can be calculated from the stretch and is defined as [40]

$$\mathbf{E}_{log} = \mathbf{P} \cdot ln\boldsymbol{\Lambda} \cdot \mathbf{P}^T \tag{3}$$

where $\mathbf{P}$ and $\boldsymbol{\Lambda}$ are, respectively, the matrices of the eigenvectors and eigenvalues of the stretch, $\mathbf{U}$. The stress, $\boldsymbol{\sigma}$, is then calculated using Hooke's law and $\mathbf{C^d}$.

In this approach, the damaged stiffness tensor follows the material rotation in the deformed situation as the stress–strain measure is derived for the current configuration and nodal positions. The CDM model with this implementation is referred to as *CDM-SS* and is compared to *CDM3D* in this study.

2.3.2. CDM-LD: Approach accounting for large deformation kinematics

The large deformation approach [41] is based on a Lagrangian kinematic measure where the constitutive equations can be defined within a orthonormal material frame. The Green–Lagrange strain, $\mathbf{E}_{GL}$, is determined from the deformation gradient tensor, $\mathbf{F}$:

$$\mathbf{E}_{GL} = \frac{1}{2}\left(\mathbf{F}^{\top} \cdot \mathbf{F} - \mathbf{I}\right) \tag{4}$$

where $\mathbf{I}$ is the identity tensor. The 2nd Piola–Kirchhoff stress, $\mathbf{S}$, can be determined from $\mathbf{E}_{GL}$ and $\mathbf{C}^d$:

$$\mathbf{S} = \mathbf{C}^d : \mathbf{E}_{GL} \tag{5}$$

$\mathbf{S}$ can be mapped to the current configuration by

$$\boldsymbol{\tau} = \mathbf{F} \cdot \mathbf{S} \cdot \mathbf{F}^T \text{ and } \boldsymbol{\sigma} = \frac{1}{J}\boldsymbol{\tau} \text{ with } J = \det(\mathbf{F}) \tag{6}$$

where $\boldsymbol{\tau}$ is the Kirchhoff stress. The stresses need to be rotated back to the co-rotational basis of Abaqus through the use of a rotation matrix, $\mathbf{R}$.

$$\boldsymbol{\sigma}_{abq} = \mathbf{R} \cdot \boldsymbol{\sigma} \cdot \mathbf{R}^T \tag{7}$$

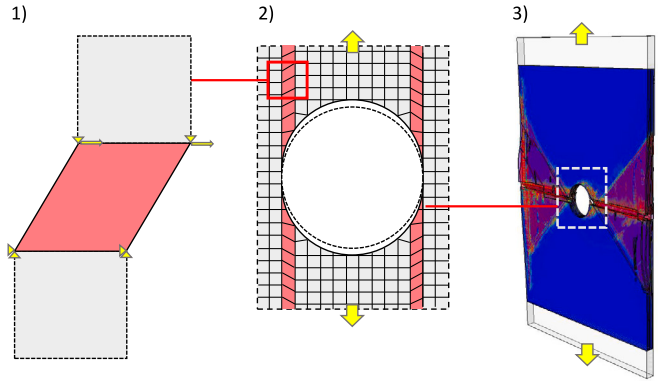

Fig. 4. Benchmarks at three different levels: (1) Single element simple shear; (2) Splitting of an open-hole UD ply and (3) Open-hole tension of a composite laminate coupon.

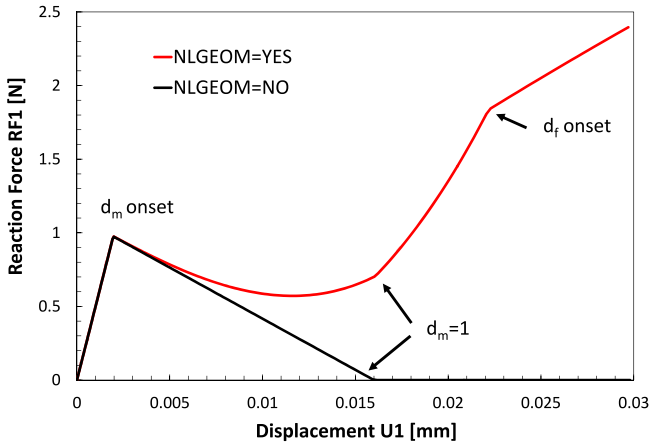

Fig. 5. Single element reaction force (RF1), simple shear loading, Abaqus build-in Hashin material model.

In this approach, the stress–strain measure used for the calculation of damage is derived based on the reference configuration. The CDM model with this implementation is referred to here as *CDM-LD* and is compared to *CompDam*.

3. Numerical analysis and discussion

The different methodologies described in Section 2 are applied to geometrically nonlinear problems involving large shear deformation, and the effect of each methodology is analyzed in this section. The models are evaluated at three different levels as shown in Fig. 4: (1) Single element simple shear; (2) Splitting of an open-hole UD ply; and (3) Open-hole tension of a composite laminate coupon. The benchmarks are chosen so that the influence of the differences in methodology can be highlighted at each level under loading conditions that are representative for ply splitting. Both the single element and open-hole UD ply benchmark are loaded in fiber direction (material axis 1) as shown in Fig. 3.

The benchmark at the single element and UD ply level follow the modeling approach described in Leone [25]. The high-fidelity modeling of the open-hole coupon takes into account both inter- and intralaminar damage, where ply-by-ply modeling is employed. The interlaminar behavior is modeled through the general contact algorithm available in Abaqus/Explicit [30], which accounts for the kinematics of surface contact, cohesive separations and friction [15,16].

For some of the studies presented in this section, the influence of linear shear (*LS*) versus nonlinear shear (*NLS*) is investigated.

3.1. Material properties

The material properties for AS4/8552 and IM7/8552 used in this study are given in Table 1. Only the properties relevant for the benchmarks are shown, while the full set is provided in Falcó et al. [16] and Leone et al. [29].

3.2. Single element simple shear

An eight-node C3D8R solid single element is loaded in simple shear as shown in Fig. 3. The size of the element is 0.1 mm in each direction and the AS4/8552 material properties are given in Table 1. The fiber direction is aligned with the 1-direction. The bottom 4 nodes are constrained in all directions, while the top nodes are constrained in 2 and 3-direction. The element is loaded at the top nodes in 1-direction by an applied displacement of 0.1 mm. The softening of the single element is studied by summing the reaction forces in 1-direction of the top nodes. The shear stress and strain provided by Abaqus is not reported here because they are provided in the rotated material direction. If the user is not aware of this material axis rotation, the softening behavior appears to be as expected in material direction stress/strain, however not in terms of stress based on the reaction forces. The expected response is linear-elastic before the onset of damage ($d_m = 0$) followed by linear softening until the reaction force reaches zero ($d_m = 1$).

The results of the single element analysis is shown in Fig. 5. The Abaqus built-in Hashin material model is used first. The influence of the material axis rotation as illustrated in Fig. 3 on the reaction forces in 1-direction during a geometrically nonlinear problem (NLGEOM=YES) is compared to the results of a linear analysis (NLGEOM=NO). Both models show identical response during the linear-elastic part and onset of damage is predicted at the same point. However, the softening response shows very different results. During the softening of the geometrically nonlinear analysis, the reaction force starts picking up load in the 1-direction due to the rotation of the material axis and incorrectly defined crack plane. Furthermore, the incorrectly defined material coordinate system also results in the development of spurious stresses. For example, the stress in fiber direction rapidly increases and results in the onset of compressive fiber damage (d_f onset) at large shear strains.

The single element model is further studied using the different approaches and the results are compared against *CDM3D* and *CompDam* in Fig. 6 during a geometrical nonlinear analysis (NLGEOM=YES). It is shown that *CDM3D* and *CDM-SS*, which do not account for material axis rotation, show the same softening response as the Hashin model (Fig. 5) with a slight difference in the onset of fiber failure due to the difference in failure criteria. However, the softening response of *CompDam* and *CDM-LD* is correct. The only difference between the models is the implementation of the softening law, which is linear in *CompDam* and exponential in the other models.

The development of spurious stresses, and ultimately compressive fiber failure (d_f) at large shear strains is also predicted by the models that do not account for material axis rotation (*CDM3D* and *CDM-SS*). Furthermore, a compressive force increases during shear loading as shown in Fig. 7, while the transverse force resulting from shear damage predicted by *CompDam* and *CDM-LD* is negligible. It should be noted that when using *CDM-LD* or *CompDam* in a geometrically linear analysis with NLGEOM=NO, the stresses are over-rotated, which causes a similarly incorrect load-transfer across the element.

3.3. Unidirectional single ply open-hole tension specimen

The second evaluation of CDM models in the present study concerns their ability to predict fiber splits in a UD single ply open-hole specimen

Table 1
Material properties of AS4/8552 [16] and IM7/8552 [29].

Property	Description	AS4/8552	IM7/8552	Unit
E_{11}	Young's modulus, longitudinal tensile direction	137 100	171 420	MPa
E_{22}	Young's modulus, transverse tensile direction	9456	9401	MPa
G_{12}	Shear modulus	4992	5290	MPa
ν_{12}	Poisson ratio, 1–2	0.314	0.32	–
ν_{23}	Poisson ratio, 2–3	0.487	0.52	–
Y_T	Mode I matrix strength	74.2	80.0	MPa
S_L	Mode II matrix strength	97.53	92.3	MPa
X_T	Fiber tensile strength	2106.4	2326.2	MPa
G_{Ic}	Mode I interlaminar fracture toughness	0.3	0.3	kJ/m^2
G_{IIc}	Mode II interlaminar fracture toughness	0.78	0.788	kJ/m^2
η	Benzeggagh–Kenane coefficient	1.45	1.634	–
G_{XT}	Longitudinal tensile fracture toughness	125	133.3	kJ/m^2

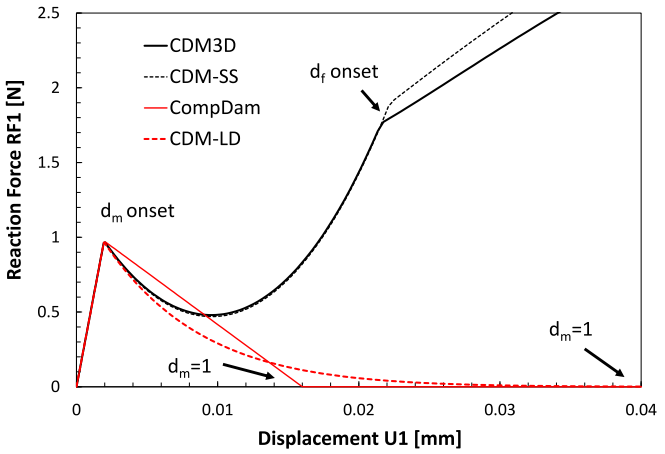

Fig. 6. Single element simple shear loading, comparing the reaction force (RF1) of the different models during geometrical nonlinear analysis (NLGEOM=YES).

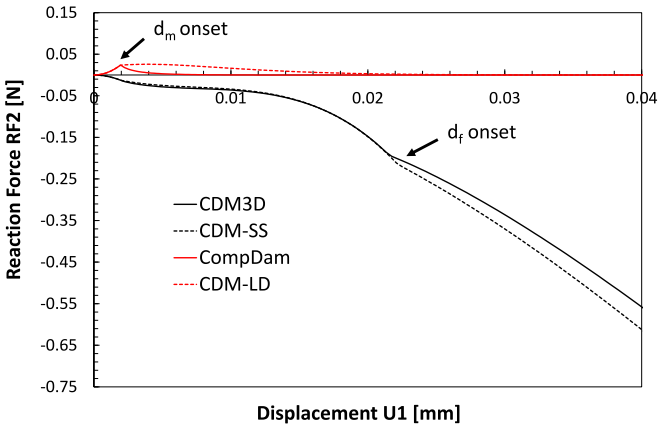

Fig. 7. Single element simple shear loading, comparing the reaction force (RF2) of the different models during geometrical nonlinear analysis (NLGEOM=YES).

following the benchmark in Leone et al. [29]. This benchmark is chosen because it shows how fiber splitting influences the stress-concentration around the hole and failure mode of the UD single ply open-hole specimen [20]. The prediction of fiber splitting is difficult because of the large shear deformation that occurs near the hole after onset of matrix damage as shown in Fig. 3. The UD open-hole model is shown in Fig. 8 and is 50.8 mm long, 12.7 mm wide with a hole of 3.175 mm in diameter. Only a single ply is modeled, meaning the thickness of the specimen is 0.183 mm. The modeling strategy follows the approach defined in Falcó et al. [16] with a fiber aligned mesh. The expected failure mode of the UD open-hole specimen is a net-section fiber failure

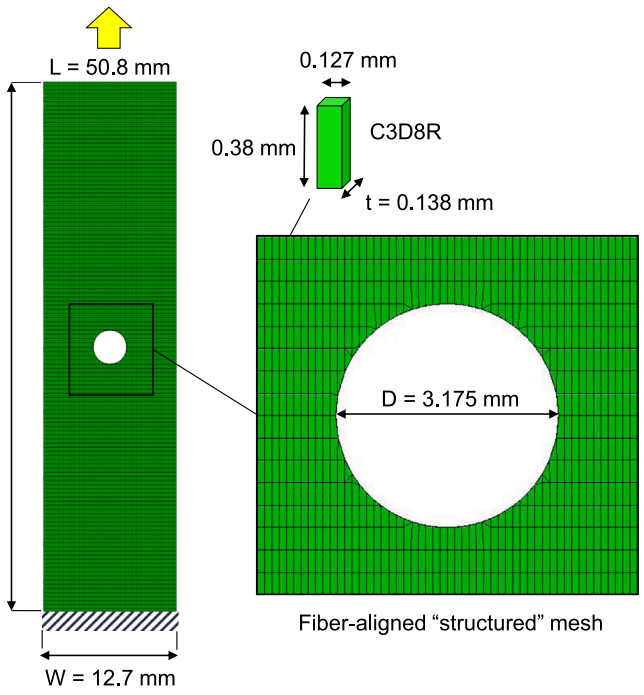

Fig. 8. Unidirectional single ply open-hole tension model, following dimensions from Leone [25].

of the remaining ligaments after the stress-concentration of the hole has been reduced by fiber splitting. The fibers are aligned with the loading direction and a fiber-aligned structural mesh is used. The elements are 0.127 mm in the transverse direction and have an aspect ratio of 3 in the longitudinal direction, resulting in an element length of 0.38 mm. The element size is chosen such that they meet the requirements for mesh regularization without experiencing snap-back behavior during softening [16]. The IM7/8552 material properties used in this study are given in Table 1.

The theoretical UD net-section strength of the open-hole specimen without stress concentration is $X_T \cdot (W - D) \cdot t_{ply} = 4054$ N. The prediction of the load–displacement curve, during a geometrical nonlinear (NLGEOM=YES) analysis, for both the *CDM3D* and *CompDam* model is shown in Fig. 9. The prediction of the initial stiffness and onset of fiber splitting (1) is very similar between the models. The *CDM3D* model, which does not account for material rotation, is unable to reduce the stress concentration at the hole. As soon as the shear deformation within the splits becomes large enough to trigger spurious failure modes the load–displacement curve drops (2) and the *CDM3D* specimen fails (3). In contrast, the *CompDam* model exhibits fully developed fiber splits from end to end (2) which greatly reduces the stress concentration such that the central region carries no load (4). As expected, final

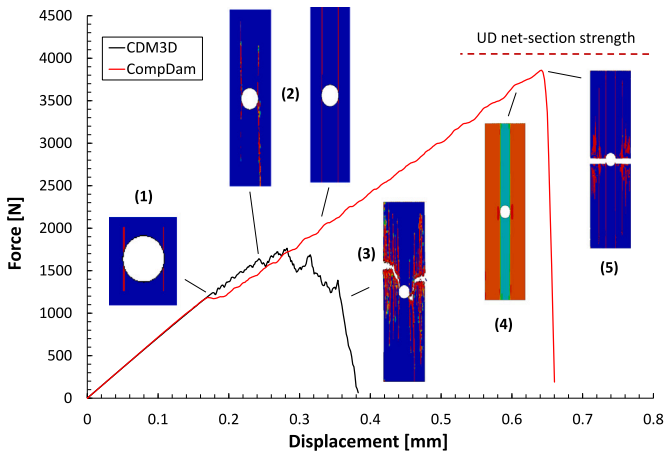

Fig. 9. Load–displacement curves of the UD open-hole ply split benchmark with comparison of difference in failure modes between *CDM3D* and *CompDam* model.

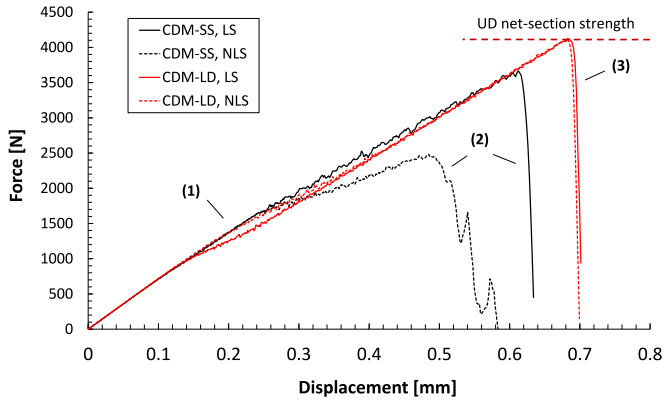

Fig. 10. Prediction of UD open-hole ply splitting, linear versus nonlinear shear using the two different approaches. The failure modes at three points are compared in Fig. 11.

failure of the specimen (5) is governed by fiber failure in the remaining ligaments. The colors in Fig. 9 (1), (2), (3) and (5) represent element damage (blue = undamaged, red = fully damaged), while the colors in (4) indicate the amount of stress carried by the ligaments related to the UD net-section strength.

The benchmark is repeated with *CDM-SS* and *CDM-LD* to investigate how the difference in methodology affects the prediction of fiber splits and final failure of the UD open-hole specimen. In addition, the effect of shear non-linearity is investigated. The load–displacement predictions are shown in Fig. 10 and the corresponding failure modes are presented in Fig. 11.

The initial linear-elastic response of the load–displacement curve is identical for both models up to the onset of matrix failure and fiber splitting. For the *CDM-SS* model (which does not account for material rotation), the inclusion of nonlinear shear in the analysis slows the development of the splits (1) and promotes the development of spurious failure modes causing early failure of the specimen (2). For *CDM-LD*, there is no significant impact of material nonlinearity on final specimen strength (3) and ply splitting is accurately captured. During the analysis, failure onset during shear loading is defined at 5% shear strain, which is a typical value for thermoset composites [27]. The introduction of nonlinear shear in the analysis showed a significant effect on the strength prediction and failure mechanics. Therefore, it becomes apparent that the effect of these spurious failure modes may play an important role in the final failure modes at laminate level and could be especially important for materials such as thermoplastic composites, which allow for even higher deformations within the local failure modes.

3.4. Open-hole tension laminate

The previous section clearly demonstrates that, to predict fiber splitting on unidirectional plies, it is necessary to account for large deformation kinematics. In this section, the effect of the modeling approaches is evaluated in the case of a multi-directional laminate typical of applications in the aerospace industry. The open-hole tension specimen of the hard laminate presented in Falcó et al. [16] is chosen for this study and is referred to as [50/40/10], which stands for the percentage of 0-, ± 45- and 90-degree plies. Fiber failure is modeled differently between the models and the (3D vs 2D) failure criteria. Also, the shape of the cohesive law for fiber failure has a pronounced effect on the coupon strength at laminate level, which is not part of the current study. Therefore, only matrix damage and delamination is compared between the models and no load–displacement curves are shown. The finite element model of the open-hole tension laminate is shown in Fig. 12 and is 38.1 mm wide, 65 mm long and has a hole with a diameter of 6.35 mm. The laminate consists of 20 plies ($[0/45/0/90/0/-45/0/45/0/-45]_s$).

The modeling strategy follows the approach defined in [15,16] and each ply consists of a fiber aligned mesh. The interlaminar behavior is modeled through the general contact algorithm available in ABAQUS/Explicit [30] to solve the issues of the non-coincident fiber aligned mesh and takes care of the kinematics of surface contact, cohesive and frictional behavior. Interlaminar damage (delamination) is described in terms of tractions and displacements by the cohesive zone model. The model reduces the stiffness of the cohesive surface thus decreasing the traction while dissipating the fracture energy corresponding to the specific mixed-mode opening mode. Mixed-mode interaction follows the Benzeggagh–Kenane criterion [42]. The quadratic nominal stress failure criteria is used for damage initiation and based on the interlaminar strength values for each damage mode. The corresponding material properties are given in Table 1. A value of 200,000 N/mm^3 is used for the mode I penalty stiffness and the shear penalty stiffness follows Turon's equation [43]. Frictional effects are considered to be ply interface angle dependent and follows the approach and values from Lopes et al. [15] and Falcó et al. [16]. Symmetry through the thickness is used to reduce the computational cost. The material properties of each ply take into the account their in-situ strength. The load is introduced into the coupon through a 'load introduction zone' with linear-elastic properties and a 'transition zone' with increased fracture toughness in order to mitigate the influence of the boundary conditions and edge.

The prediction of the failure mode of the [50/40/10] open-hole tension test by using the CDM approaches (1: *CDM3D*, 2: *CDM-SS*) is shown in Fig. 13. As expected, the final failure of the open-hole tension test is dominated by fiber failure due to the large number of 0-degree plies. Both models predict a clean net-section failure with limited matrix damage and delaminations.

The predictions of the failure mode of the open-hole specimen by the *CompDam* and *CDM-LD* model is shown in Fig. 14. Although final failure of the coupon is still dominated by fiber failure, the development of internal matrix damage, fiber splits and their interaction with delaminations is very different compared to Fig. 13. The large difference in predicted failure modes demonstrates that accounting for large deformations appears to also be important at the laminate level as ply splitting will highly influence the development of delaminations.

A closer look at the failure mode reveals similar issues as identified by the previous described test cases. Within the matrix cracks and ply splits there are signs of spurious failure modes, which triggers incorrect failure of elements in their surrounding. A sign of compressive fiber failure using the *CDM3D* model (1) is shown in Fig. 15, while *CDM-LD* shows large shear deformation at the local scale within the

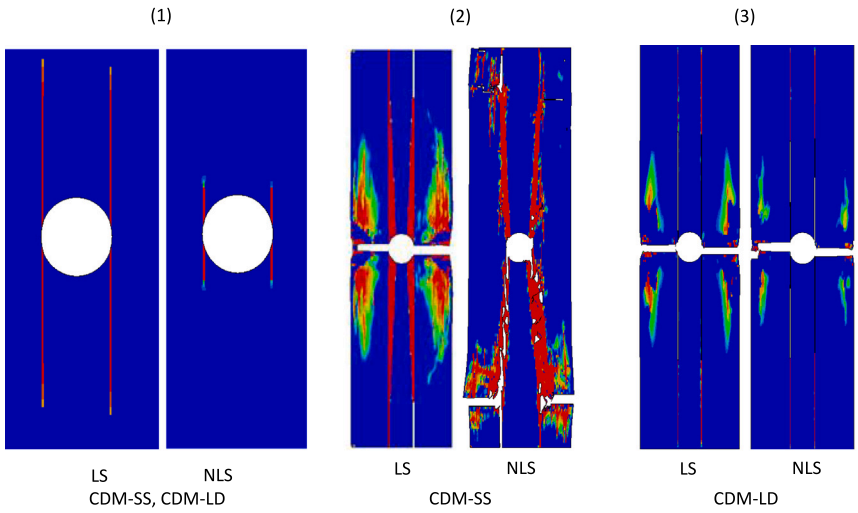

Fig. 11. Comparison of the UD open-hole failure modes from Fig. 10: (1) initiation of ply splitting; (2) *CDM-SS*, LS vs NLS; (3) *CDM-LD*, LS vs NLS.

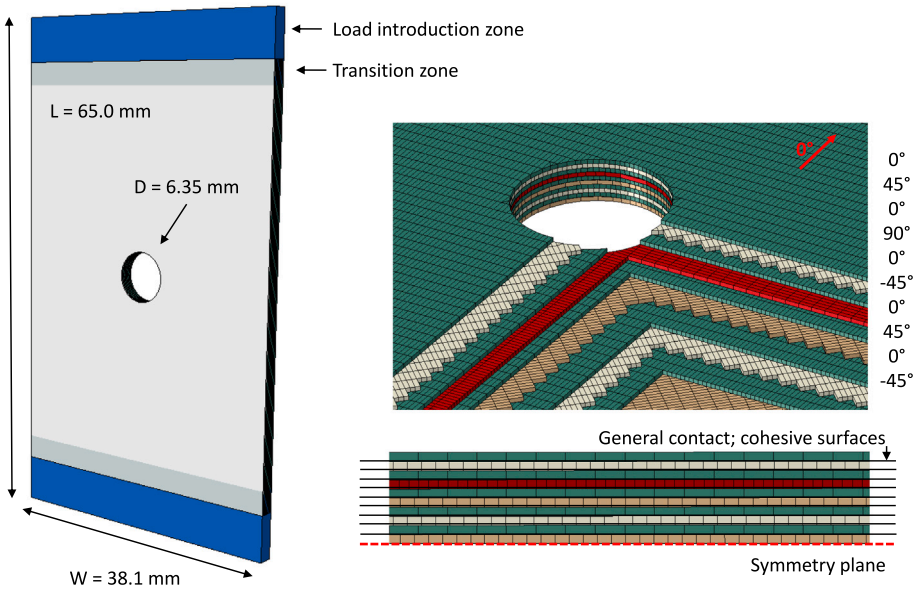

Fig. 12. Finite element model of the open-hole tension laminate specimen.

fully developed matrix splits (2). The presence of high shear strains within the splits demonstrates that it is important to account for large deformation kinetics in the constitutive model, even in the case of thermoset materials that typically fail around 5% shear deformation.

The development of matrix cracks, ply splits and their interaction is shown in Fig. 16. Matrix damage starts to develop near the edges of the hole on each ply in the direction of the fiber (1). Fiber damage initiates along the net section of the hole and delamination starts to interact with the ply splits near the hole following the 45-degree plies (2). The fibers near the hole become fully damaged and some elements are removed. A strong interaction between the ply splits and delamination is observed (3) until they reach the edges of the coupon (4). Similar internal failure modes can be observed in the experimental results and in the literature [22,23,44]. The failure mode of a [50/40/10] open-hole tension laminate is shown in Fig. 17 and the directions of ply splits are marked. The experimental data shown in Falcó et al. [16] shows a net-section failure mode, but the coupon is not fully separated. However, after full separation of a specimen from the same testing campaign, it can be concluded that internal failure modes similar to those predicted by the *CompDam* and *CDM-LD* model are present in the experimental data and that ply splits and delaminations follow the 45-degree plies.

4. Conclusion

The importance of accounting for large deformation in predictions of matrix failure of composites is demonstrated in this paper. The constitutive behavior of two recently developed continuum damage models is investigated. Two continuum damage model approaches are implemented that use different stress–strain measures. The first approach *CDM-SS* is based on small-strain increments and the Cauchy stress, while the second approach *CDM-LD* accounts for large deformation kinematics through the use of the Green–Lagrange strain and the 2nd Piola–Kirchhoff stress. The ability of the CDM models to predict matrix failure and ply splitting is evaluated by benchmarks at the single element, ply and coupon level. It is found that approaches based on small strain increments and logarithmic strains run into difficulties during large shear deformation as spurious stresses trigger incorrect failure modes. The incorrectly defined matrix crack orientation due to material axis rotation may cause load transfer across matrix cracks,

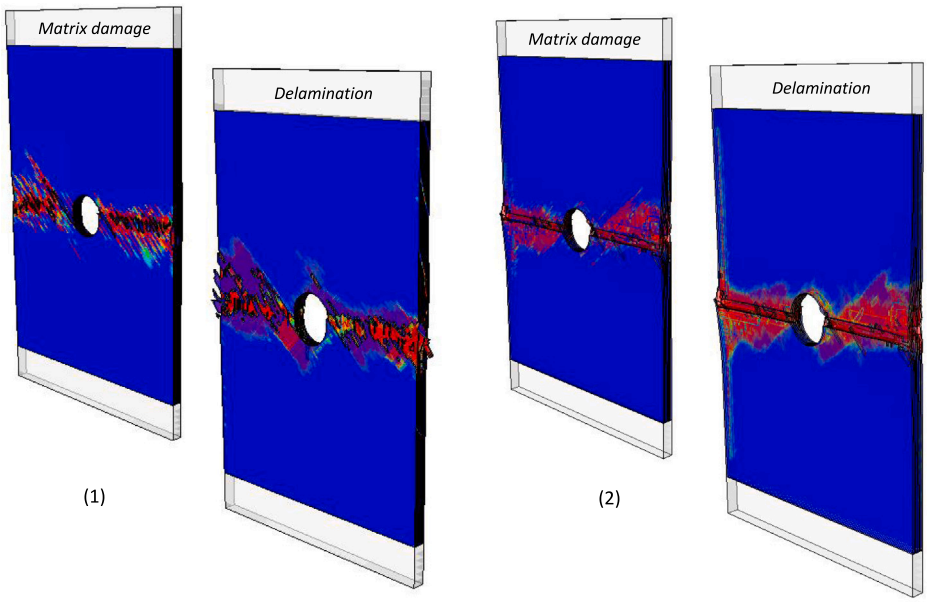

Fig. 13. Failure mode of [50/40/10] open-hole tension analysis: (1) *CDM3D*; (2) *CDM-SS*.

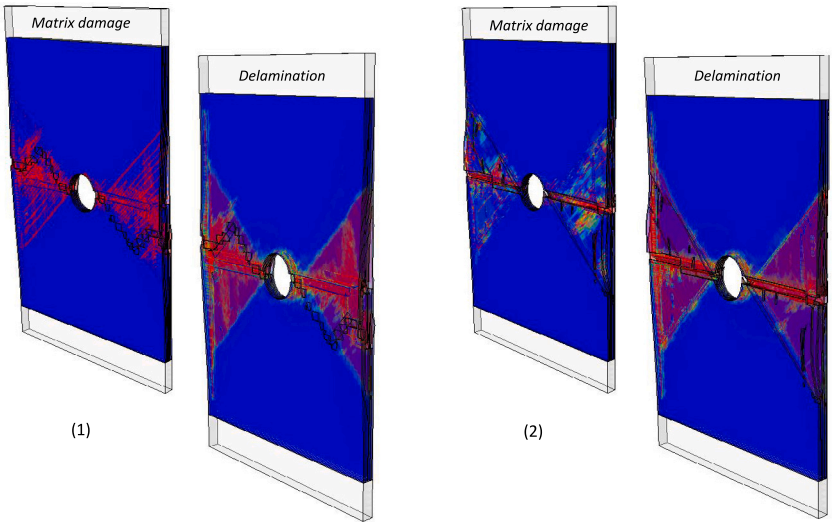

Fig. 14. Failure mode of [50/40/10] open-hole tension analysis: (1) *CompDam*; (2) *CDM-LD*.

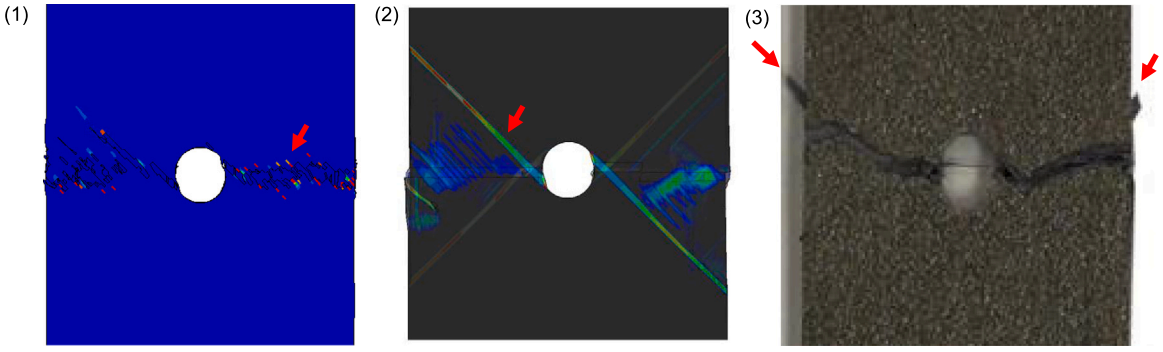

Fig. 15. Detailed look at failure mode of [50/40/10] open-hole tension analysis: (1) *CDM3D*, compressive fiber failure within matrix splits; (2) *CDM-LD*, large shear deformation (5%–50%) at the local scale within fully developed matrix splits; (3) Indication of ply splits in published experimental failure mode open-hole, adapted from Falcó et al. [16].

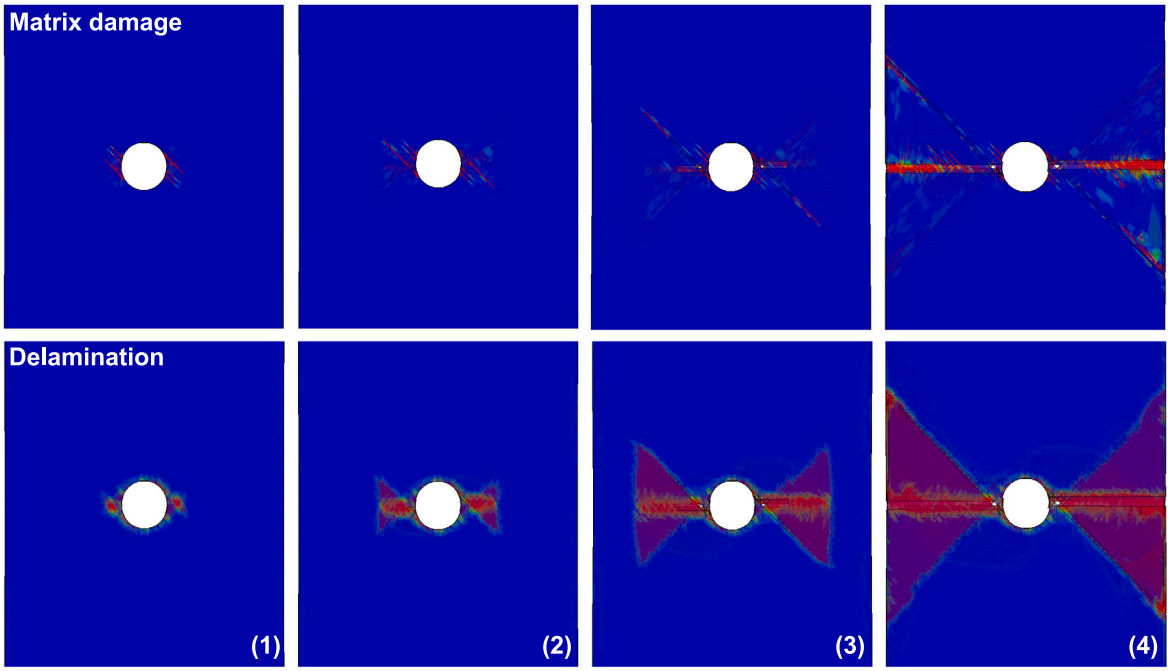

Fig. 16. Development of matrix damage, ply splits and interaction with delamination using *CDM-LD* model: (1) initiation of damage near hole edge; (2) Start of fiber damage and ply splits; (3) Propagation of ply splits and interaction with delamination; (4) Final failure mode.

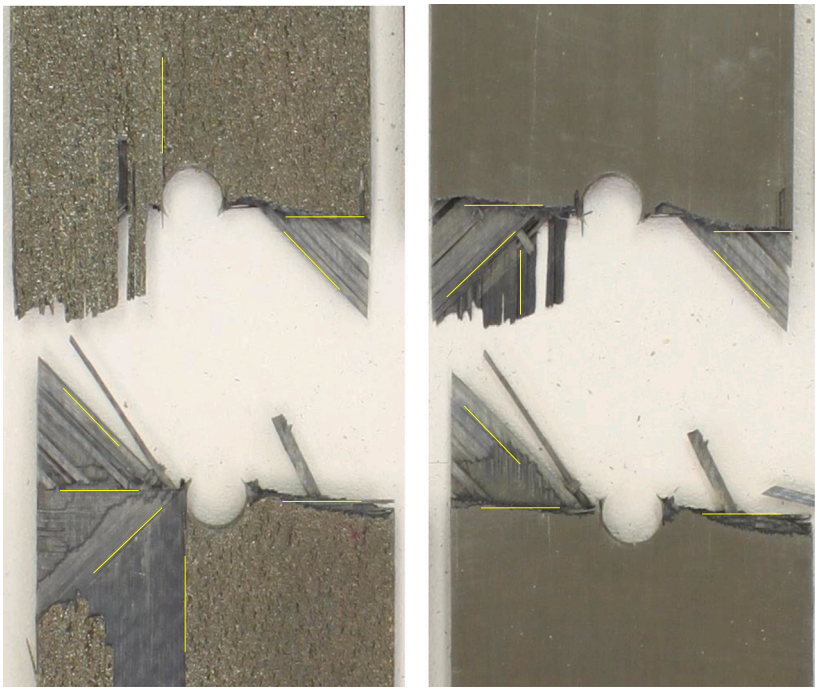

Fig. 17. Experimental failure mode of open-hole laminate after full separation of the fully failed laminates, ply split directions marked in yellow.

where the strain and/or rotations due to softening and material nonlinearity may become large enough to invalidate the assumptions inherent to small strain theory. Analysis of the open-hole laminate also confirms a CDM approach based on small-strain increments and the Cauchy stress is insufficient to predict correct failure mechanisms. For example, fiber compression failure is triggered locally and limited interactions of the fiber splits with delamination are observed. The present analysis also shows that the inaccurate failure mechanisms are corrected by expressing the constitutive equations based on a Lagrangian kinematic measure, as implemented in the *CompDam* and *CDM-LD* models. Accounting for large deformation kinematics results in the prediction of fully developed ply splits, and allows for strong interaction with delaminations, resulting in a significant improvement in the prediction of the open-hole coupon internal failure mechanisms as shown by comparison to the experimental failure mode. From the insights gained in this study, it is recommended to base CDM models on a Lagrangian kinematic measure to improve their ability to predict ply splitting. Furthermore, the improvements in the numerical methodology may also help to analyze the matrix-dominated failure modes of thermoplastic

composites welded joints as it is expected that their increased toughness and nonlinear behavior will promote larger deformations in the local failure mechanisms.

CRediT authorship contribution statement

B.H.A.H. Tijs: Conceptualization, Methodology, Software, Investigation, Validation, Writing – original draft, Writing – review & editing. **C.G. Dávila:** Conceptualization, Methodology, Writing – review. **A. Turon:** Supervision, Conceptualization, Writing – review. **C. Bisagni:** Supervision, Conceptualization, Writing – review.

Declaration of competing interest

The authors declare that they have no known competing financial interests or personal relationships that could have appeared to influence the work reported in this paper.

Data availability

Data will be made available on request.

Acknowledgments

The authors would like to thank the journal and editors for organizing this special issue in memory of our dear friend and colleague Claudio S. Lopes and are honored to participate. In the period of 2014–2020, the first author has worked closely with Claudio as part of a collaboration between IMDEA Materials Institute and Fokker/GKN Aerospace on the VIRTEST project [15–17,45,46] to develop a simulation strategy to predict the mechanical behavior of aeronautical composites. This collaboration inspired the first author to conduct his own research as part of a PhD project at the Delft University of Technology in the same department (ASM/ASCM) where Claudio obtained is PhD degree.

The work described in this paper received co-funding from the Clean Sky 2 Joint Undertaking (JU) under grant agreement No 945583 (project STUNNING). The JU receives support from the European Union's Horizon 2020 research and innovation programme and the Clean Sky 2 JU members other than the Union.

Disclaimer

The results, opinions, conclusions, etc. presented in this work are those of the author(s) only and do not necessarily represent the position of the JU; the JU is not responsible for any use made of the information contained herein.

Specific vendor and manufacturer names are explicitly mentioned only to accurately describe the software or hardware used. The use of vendor and manufacturer names does not imply an endorsement by the corporation or U.S. Government nor does it imply that the specified equipment is the best available.

References

[1] van Ingen JW, Waleson JEA, Offringa A, Chapman M. Double curved thermoplastic orthogrid rear fuselage shell. In: SAMPE Europe conference. Nantes, France; 2019, p. 1–10.

[2] Tijs BHAH, van Dooren KS, Bisagni C. Development of a numerical framework for virtual testing to support design of a next generation thermoplastic multifunctional fuselage. In: European conference on multifunctional structures (EMuS2020), November, 17-18, 202. Scipedia, S.L.; 2020, p. 90–5. http://dx.doi.org/10.23967/EMUS.2020.005.

[3] Tijs BHAH, Doldersum MHJ, Turon A, Waleson JEA, Bisagni C. Experimental and numerical evaluation of conduction welded thermoplastic composite joints. Compos Struct 2022;281:114964. http://dx.doi.org/10.1016/J.COMPSTRUCT.2021.114964.

[4] Tijs BHAH, Abdel-Monsef S, Renart J, Turon A, Bisagni C. Characterization and analysis of the interlaminar behavior of thermoplastic composites considering fiber bridging and R-curve effects. Composites A 2022;162:107101. http://dx.doi.org/10.1016/J.COMPOSITESA.2022.107101.

[5] Wisnom MR, Chang F-K. Modelling of splitting and delamination in notched cross-ply laminates. Compos Sci Technol 2000;60(15):2849–56. http://dx.doi.org/10.1016/S0266-3538(00)00170-6.

[6] Iarve EV, Mollenhauer DH. Mesh-independent matrix cracking and delamination modeling in advanced composite materials. In: Numerical modelling of failure in advanced composite materials. Woodhead Publishing; 2015, p. 227–64. http://dx.doi.org/10.1016/B978-0-08-100332-9.00009-8.

[7] Le MQ, Bainier H, Néron D, Ha-Minh C, Ladevèze P. On matrix cracking and splits modeling in laminated composites. Composites A 2018;115:294–301. http://dx.doi.org/10.1016/J.COMPOSITESA.2018.10.002.

[8] Nguyen MH, Waas AM. Modeling delamination migration in composite laminates using an enhanced semi-discrete damage model (eSD2M). Int J Solids Struct 2022;236–237:111323. http://dx.doi.org/10.1016/J.IJSOLSTR.2021.111323.

[9] Huang J, Zhang C, Wang J, Zhang C. On the applicability of rate-dependent cohesive zone models in low-velocity impact simulation. Eng Fract Mech 2022;271:108659. http://dx.doi.org/10.1016/j.engfracmech.2022.108659.

[10] Camanho PP, Bessa MA, Catalanotti G, Vogler M, Rolfes R. Modeling the inelastic deformation and fracture of polymer composites-part II: Smeared crack model. Mech Mater 2013;59:36–49. http://dx.doi.org/10.1016/j.mechmat.2012.12.001.

[11] Van der Meer FP, Moës N, Sluys LJ. A level set model for delamination - modeling crack growth without cohesive zone or stress singularity. Eng Fract Mech 2012;79:191–212. http://dx.doi.org/10.1016/j.engfracmech.2011.10.013.

[12] Hallett SR, Harper PW. Modelling delamination with cohesive interface elements. In: Numerical modelling of failure in advanced composite materials. Elsevier Inc.; 2015, p. 55–72. http://dx.doi.org/10.1016/B978-0-08-100332-9.00002-5.

[13] Chen BY, Pinho ST, De Carvalho NV, Baiz PM, Tay TE. A floating node method for the modelling of discontinuities in composites. Eng Fract Mech 2014;127:104–34. http://dx.doi.org/10.1016/j.engfracmech.2014.05.018.

[14] Maimí P, Camanho PP, Mayugo JA, Dávila CG. A continuum damage model for composite laminates: Part II - computational implementation and validation. Mech Mater 2007;39(10):909–19. http://dx.doi.org/10.1016/j.mechmat.2007.03.006.

[15] Lopes CS, Gómez DG, Falcó O, Tijs BHAH. Stochastic virtual testing laboratory for unidirectional composite coupons: from conventional to dispersed-ply laminates. In: Multi-scale continuum mechanics modelling of fibre-reinforced polymer composites. Elsevier; 2021, p. 579–607. http://dx.doi.org/10.1016/b978-0-12-818984-9.00019-6.

[16] Falcó O, Ávila RL, Tijs B, Lopes CS. Modelling and simulation methodology for unidirectional composite laminates in a virtual test lab framework. Compos Struct 2018;190:137–59. http://dx.doi.org/10.1016/j.compstruct.2018.02.016.

[17] Falcó O, Lopes CS, Sommer DE, Thomson D, Ávila RL, Tijs BHAH. Experimental analysis and simulation of low-velocity impact damage of composite laminates. Compos Struct 2022;287:115278. http://dx.doi.org/10.1016/J.COMPSTRUCT.2022.115278.

[18] Wisnom MR, Khan B, Hallett SR. Size effects in unnotched tensile strength of unidirectional and quasi-isotropic carbon/epoxy composites. Compos Struct 2008;84(1):21–8. http://dx.doi.org/10.1016/J.COMPSTRUCT.2007.06.002.

[19] Kortschot MT, Beaumont PW. Damage mechanics of composite materials: I—measurements of damage and strength. Compos Sci Technol 1990;39(4):289–301. http://dx.doi.org/10.1016/0266-3538(90)90077-I.

[20] Iarve EV, Mollenhauer D, Kim R. Theoretical and experimental investigation of stress redistribution in open hole composite laminates due to damage accumulation. Composites A 2005;36(2):163–71. http://dx.doi.org/10.1016/J.COMPOSITESA.2004.06.011.

[21] Mollenhauer D, Iarve EV, Kim R, Langley B. Examination of ply cracking in composite laminates with open holes: A moiré interferometric and numerical study. Composites A 2006;37(2):282–94. http://dx.doi.org/10.1016/J.COMPOSITESA.2005.06.004.

[22] Hallett SR, Green BG, Jiang WG, Wisnom MR. An experimental and numerical investigation into the damage mechanisms in notched composites. Composites A 2009;40(5):613–24. http://dx.doi.org/10.1016/J.COMPOSITESA.2009.02.021.

[23] Nikishkov Y, Makeev A, Seon G. Simulation of damage in composites based on solid finite elements. J Am Helicopter Soc 2010;55(4):042009. http://dx.doi.org/10.4050/JAHS.55.042009.

[24] Llobet J, Maimí P, Turon A, Bak BL, Lindgaard E, Carreras L, et al. A continuum damage model for composite laminates: Part IV- experimental and numerical tests. Mech Mater 2021;154:103686. http://dx.doi.org/10.1016/J.MECHMAT.2020.103686.

[25] Leone FA. Deformation gradient tensor decomposition for representing matrix cracks in fiber-reinforced materials. Composites A 2015;76:334–41. http://dx.doi.org/10.1016/j.compositesa.2015.06.014.

[26] Fallahi H, Taheri-Behrooz F, Asadi A. Nonlinear mechanical response of polymer matrix composites: A review. Polym Rev 2020;60(1):42–85. http://dx.doi.org/10.1080/15583724.2019.1656236.

[27] Lafarie-Frenot M, Touchard F. Comparative in-plane shear behaviour of long-carbon-fibre composites with thermoset or thermoplastic matrix. Compos Sci Technol 1994;52(3):417–25. http://dx.doi.org/10.1016/0266-3538(94)90176-7.

[28] Carlsson LA, Gillespie JW, Trethewey BR. Mode II interlaminar fracture of graphite/epoxy and graphite/PEEK. J Reinf Plast Compos 1986;5(3):170–87. http://dx.doi.org/10.1177/073168448600500302.
[29] Leone FA, Bergan AC, Dávila CG. CompDam - deformation gradient decomposition (DGD). 2019, URL https://github.com/nasa/CompDam_DGD.
[30] SIMULIA Dassault Systemes. ABAQUS user's manual, version 2019. 2019.
[31] Catalanotti G, Camanho PP, Marques AT. Three-dimensional failure criteria for fiber-reinforced laminates. Compos Struct 2013;95:63–79. http://dx.doi.org/10.1016/j.compstruct.2012.07.016.
[32] Maimí P, Camanho PP, Mayugo JA, Dávila CG. A continuum damage model for composite laminates: Part I - constitutive model. Mech Mater 2007;39(10):897–908. http://dx.doi.org/10.1016/j.mechmat.2007.03.005.
[33] Dávila CG, Rose CA, Camanho PP. A procedure for superposing linear cohesive laws to represent multiple damage mechanisms in the fracture of composites. Int J Fracture 2009;158(2):211–23. http://dx.doi.org/10.1007/S10704-009-9366-Z.
[34] Puck A, Schürmann H. Failure analysis of FRP laminates by means of physically based phenomenological models. Compos Sci Technol 1998;58(7):1045–67. http://dx.doi.org/10.1016/S0266-3538(96)00140-6.
[35] Puck A, Kopp J, Knops M. Guidelines for the determination of the parameters in Puck's action plane strength criterion. Compos Sci Technol 2002;62(3):371–8. http://dx.doi.org/10.1016/S0266-3538(01)00202-0.
[36] Knops M. Analysis of failure in fiber polymer laminates: the theory of alfred puck. Springer Berlin Heidelberg; 2008, p. 1–205. http://dx.doi.org/10.1007/978-3-540-75765-8.
[37] VDI-2014 blatt 3: Entwicklung von bauteilen aus faser-kunststoff-verbund - berechnungen. 2006.
[38] Bažant ZP, Oh BH. Crack band theory for fracture of concrete. Matériaux et Constructions 1983;16(3):155–77. http://dx.doi.org/10.1007/BF02486267.
[39] Tan W, Falzon BG, Price M. Predicting the crushing behaviour of composite material using high-fidelity finite element modelling. Int J Crashworthiness 2015;20(1):60–77. http://dx.doi.org/10.1080/13588265.2014.972122.
[40] Batra RC. Elements of continuum mechanics. Reston, VA: American Institute of Aeronautics and Astronautics; 2006, http://dx.doi.org/10.2514/4.861765.
[41] Holzapfel GA. Nonlinear solid mechanics: A continuum approach for engineering. West Sussex, England: John Wiley & Sons Lt.; 2000.
[42] Benzeggagh ML, Kenane M. Measurement of mixed-mode delamination fracture toughness of unidirectional glass/epoxy composites with mixed-mode bending apparatus. Compos Sci Technol 1996;56(4):439–49. http://dx.doi.org/10.1016/0266-3538(96)00005-X.
[43] Turon A, Camanho PP, Costa J, Renart J. Accurate simulation of delamination growth under mixed-mode loading using cohesive elements: Definition of interlaminar strengths and elastic stiffness. Compos Struct 2010;92(8):1857–64. http://dx.doi.org/10.1016/j.compstruct.2010.01.012.
[44] Wisnom MR. The role of delamination in failure of fibre-reinforced composites. Phil Trans R Soc A 2012;370(1965):1850–70. http://dx.doi.org/10.1098/rsta.2011.0441.
[45] Lopes C, González C, Falcó O, Naya F, LLorca J, Tijs B. Multiscale virtual testing: the roadmap to efficient design of composites for damage resistance and tolerance. CEAS Aeronaut J 2016;7(4). http://dx.doi.org/10.1007/s13272-016-0210-7.
[46] Baluch AH, Falcó O, Jiménez J, Tijs BHAH, Lopes CS. An efficient numerical approach to the prediction of laminate tolerance to barely visible impact damage. Compos Struct 2019;225. http://dx.doi.org/10.1016/j.compstruct.2019.111017.